International Journal of Mechanical and Production Engineering Research and Development (IJMPERD)
ISSN(P): 2249-6890; ISSN(E): 2249-8001
Vol. 9, Issue 2, Apr 2019, 349-360

SWCNTs - WATER ON CARREAU MHD FLOW UP A WALL WITH DISTINCT THICKNESS

JAAFAR ABDUL ABBAS ABBOOD AL-NASRAWI, ROZAINI BIN ROSLAN, R. KANDASAMY, INAS R. ALI & RADIAH MOHAMAD

Faculty of Applied Sciences and Technology,

Universiti Tun Hussein Onn Malaysia, Parit Raja, Batu Pahat, Johor, Malaysia

ABSTRACT

This study was conducted to investigate the effects of several parameters in the Navier - Stokes equations describing the nanofluid flow subjected to different electric fields. The boundary layer of SWCNTs – water flow over a stretched surface of different thicknesses in the presence of weak and strong electric fields was analyzed. The governing equations were essentially a set of ordinary differential equations (ODEs), solved using the R.K Fehlberg method with shooting technique (via MAPLE 18 software). The positive correlation between electric field and temperature was rather significant. The mass transfer rate increased with respect to most of the working parameters, indicating that the mass transfer is dominated in the presence of electric field with stretching sheet in different variables.

KEYWORDS: MHD Carreaunanofluid Flow, Single Walled Carbon Nanotube, The Thermal Conductivity, Electric Field, Stretching Sheet With Deferent Variables & Shooting with Rungekutta Method

Received: Dec 23, 2018; **Accepted:** Jan 13, 2019; **Published:** Feb 27, 2019; **Paper Id.:** IJMPERDAPR201934

Original Article

NOMENCLATURE

$B(x) = B_0(x+b)^{\frac{1-m}{2}}$ **:** Magnetic field factor

σ **:** Electrical conductivity

$E(x) = E_0(x+b)^{\frac{1-m}{2}}$: Electrical field factor

u, v : x- and y- velocity

C_w : Wall concentration

C_∞ : Ambient concentration of the nanofluid

T : Nanofluid temperature

C :Nanofluid concentration

ρ_{nf} : Nanofluid effective density

α_{nf} : Nanofluid thermal diffusivity

μ_{nf} : Nanofluid dynamic viscosity

$(\rho c_p)_{nf}$: Nanofluid heat capacitance

1. INTRODUCTION

The thermal conductivity of nano refrigerant increases significantly with respect to its volume fraction, [1]. In this research, the volume space formation of nanoparticle cluster in fluid was fabricated and the impact of the thickness of the intake sheet of nanoparticles was studied [2]. The formation of the single walled carbon nanotube could be regarded as a single smoothie, curved up graphene sheet. The graphene sheet contains sextuple grids of carbon atoms. Single walled carbon nanotube (CNT) contains of a single graphene sheet with exemplary diameter 1.0 -1.5 nm. On the other hand, multi-walled (CNT) (MWCNT) contains many graphene sheets with thickness curved up one inside. The typical diameter of (CNT) is very much dependent on the size of the impetus particles used to produce the (CNT)[3-7].SWCNTs-water has been used in nano biological gadgets and nano mechanical frameworks, [8-12]. They are generally adopted to improve the solubility. Meanwhile they can be stabilized by a surfactant within the base fluid to prevent agglomeration and sedimentation[13-14]. Several researchers including [15-17] have used nanofluids to improve heat transfer in thermal system of different geometries subjected to different thermal boundary. Some related studies in micro channels have been conducted as well[18-27]. Thermal radiation energy due to SWCNTs on MHD nanofluid flow in the presence of seawater/water: Lie group transformation, [28].

The aim of the current work was to study the mathematical scheme used to analyze the Carreau SWCNTs - water nanofluid flow due to nonlinear stretching sheet with extensible thickness. However, there have been no controlled studies, comparing the differences between the work in (Khan, Mair et. al 2017) and our previous work in simulating Carreau SWCNTs - water nanofluid flow due to nonlinear stretching sheet with extensible thickness [29].

2. BASIC EQUATIONS

The aim of this study was to clarify several aspects of the mathematical equation used to study the Carreau SWCNTs – water nanofluid flow due to the nonlinear stretching sheet with extensible thickness. The sheet was developed with velocity $U_w = U_o(x+b)^m$, where U_0 is the source velocity. $B(x+b)^{\frac{1-m}{2}}$, is the thickness of sheet and b is the dimensionless constant, m is the power law index. It was known earlier that the model must be pleased only for $m \neq 1$, as the model reduces to using flat sheet as for $m = 1$. The flexible magnetic field strength $B_0(x)$ was imposed vertically to the plate. The electric and magnetic fields were acting perpendicular to the surface.

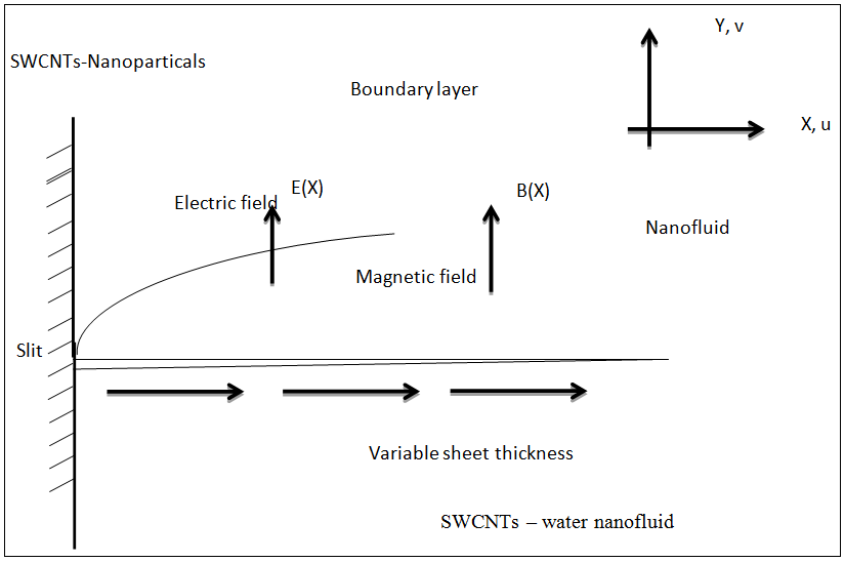

Figure 1: Physical Configuration of SWCNTs – Water Nanofluid System

Equation (1) is the continuity equation where the current function is used to describe the x- and y- velocities.

$$\frac{\partial u}{\partial x}=-\frac{\partial v}{\partial y} \tag{1}$$

$$u\frac{\partial u}{\partial x}+v\frac{\partial u}{\partial y}=\frac{\mu_{nf}}{\rho_{nf}}\left(\frac{\partial^2 u}{\partial y^2}+\frac{3\,(n-1)}{2}\Gamma^2\left(\frac{\partial u}{\partial y}\right)^2\frac{\partial^2 u}{\partial y^2}\right)-\frac{\sigma_{nf}}{\rho_{nf}}\left(E(x)B(x)-B_0^2(x)u\right) \tag{2}$$

$$u\frac{\partial T}{\partial x}+v\frac{\partial T}{\partial y}=\frac{k_{nf}}{(\rho c_p)_{nf}}\left(\frac{\partial^2 T}{\partial y^2}\right)-\frac{1}{(\rho c_p)_{nf}}\frac{\partial q_r}{\partial y}+\frac{1}{(\rho c_p)_{nf}}\tau\left[(D_B)_{nf}\left\{\frac{\partial C}{\partial y}\frac{\partial T}{\partial y}\right\}+\frac{(D_T)_{nf}}{T_\infty}\left\{\left(\frac{\partial T}{\partial y}\right)^2\right\}\right]+\frac{Q_0(T-T_\infty)}{(\rho c_p)_{nf}} \tag{3}$$

$$\frac{\partial C}{\partial x}+v\frac{\partial C}{\partial y}=(D_B)_{nf}\left(\frac{\partial^2\phi}{\partial y^2}\right)+\frac{(D_T)_{nf}}{T_\infty}\left\{\frac{\partial^2 T}{\partial y^2}\right\}+K(C_\infty-C) \tag{4}$$

The correlated boundary equations for stretching sheet are

$$u\left(x,B(x+b)^{(\frac{1-m}{2})}\right)=U_o(x+b)^m;\ v\left(x+B(x+b)^{(\frac{1-m}{2})}\right)=0;\ T(x+B(x+b)^{(\frac{1-m}{2})})=T_w$$

$$C\left(x+B(x+b)^{(\frac{1-m}{2})}\right)=C_w;\ u(x,\infty)\to 0;T\to T_\infty;\quad C\to C_\infty\quad as\ y\to\infty \tag{5}$$

$$\rho_{nf}=(1-\zeta)\rho_f+\zeta\rho_s,\ \mu_{nf}=\frac{\mu_f}{(1-\zeta)^{2.5}},\ (\rho\beta)_{nf}=(1-\zeta)(\rho\beta)_f+\zeta(\rho\beta)_s,\ (\rho c_p)_{nf}=(1-\zeta)(\rho c_p)_f+\zeta(\rho c_p)_s$$

$$\alpha_{nf}=\frac{k_{nf}}{(\rho c_p)_{nf}},\ \frac{k_{nf}}{k_f}=\left\{\frac{(k_s+(l-1)k_f)-(l-1)\zeta(k_f-k_s)}{(k_s+(l-1)k_f)+\zeta(k_f-k_s)}\right\},\ \sigma_{nf}=\zeta\sigma_s+(1-\zeta)\sigma_f\ \ (D_B)_{nf}=(1-\zeta)(D_B)_f \tag{6}$$

The Maxwell design method was used to assign the dynamic thermal or electrical conductivities of liquid-solid suspensions. Here, σ_f and σ_s are the electric conductivities, k_f and k_s are the thermal conductivities, ζ is the nanoparticle volume fraction, ρ_f and ρ_s are the densities, μ_f is the dynamic viscosity and k_{nf} is the effective thermal

conductivity. Note the Rosseland's dissipation for the radiative heat flux is $q_r = -\frac{4\sigma^* \partial T^4}{3k^* \partial y}$ [30]), where k^* is the Rosseland mean absorption coefficient and σ^* is the Stephen-Boltzmann constant. Finally, the term T^4 can be experded from too via Taylor's series $T^4 = 4T_\infty^3 T - 3T_\infty^4$.

via similarity conversions:

$$\psi = \sqrt{\frac{2\nu_f U_0 (x+b)^{m-1}}{m+1}} f(\eta), \eta = \sqrt{\frac{(m+1)U_0 (x+b)^{(m-1)}}{2\nu_f}} y, \theta(\eta) = \frac{T - T_\infty}{T_w - T_\infty}, \phi(\eta) = \frac{C - C_\infty}{C_w - C_\infty}, \tag{7}$$

The stream function ψ can be constructed as $u = \frac{\partial \psi}{\partial y}, v = -\frac{\partial \psi}{\partial x}$ which adequately attends the Equation (1). Depending on equations (6, 7), equation (1) is fairly influenced while the equations (2) and (4) incomes the representative of three works that will be examined, all of which

$$F'''\left(1 + \left(\frac{3(n-1)}{2} W^2 (F'')^2\right)\right) + G.B\left(\frac{2m}{m+1} F'^2 - FF''\right) + G.A.M(E_1 - F'^2) = 0 \tag{8}$$

$$\theta'' + \Pr_f .E.\left(F\theta' + (A1) Nb\, \theta'\phi' + (A1) Nt\, \theta'^2 + \lambda\theta\right) = 0 \tag{9}$$

$$\phi'' + (A1).\left(\frac{1}{(A1)} \frac{Nt}{Nb} \theta'' + LeF\theta' - Le\gamma\phi\right) = 0 \tag{10}$$

The boundary conditions are

$$(1+m)F(\alpha) = (1-m)\,\alpha, F'(\alpha) = 1, \theta(\alpha) = 1, \phi(\alpha) = 1; F'(\infty) = 0, \theta(\infty) = 0, \phi(\infty) = 0 \tag{11}$$

$$K_{nf} = (k_s + (e-1)(k_f) - (e-1)\zeta(k_f - (k_s), K_f = (k_s + (e-1)(k_f) - \zeta(k_f - (k_s), B = \left(1 - \zeta + \zeta \frac{\rho_s}{\rho_f}\right), T = \frac{K_{nf}}{K_f}, \tag{12}$$

$$E = \left(1 - \zeta + \zeta \frac{\rho_s (cp)_s}{\rho_f (cp)_f}\right), A = \left(1 + \frac{3\left(\frac{\sigma_s}{\sigma_f} - 1\right)\zeta}{\left(\frac{\sigma_s}{\sigma_f} + 2\right) - \left(\frac{\sigma_s}{\sigma_f} - 1\right)\zeta}\right), G = (1-\zeta)^{2.5}, A1 = \frac{1}{1-\zeta}$$

(13)

Here, $\alpha = B\sqrt{\frac{U_0}{2\nu_f (m+1)^{-1}}}$ is the related wall thickness parameter and $\eta = B\sqrt{\frac{U_0 (m+1)}{2\nu_f}}$ is the dependent plate surface.

Up on applying transformations, $f(\alpha) = f(\eta - \alpha) = f(\eta)$, $\theta(\alpha) = \theta(\eta - \alpha) = \theta(\eta)$, and $\phi(\alpha) = \phi(\eta - \alpha) = \phi(\eta)$,

Equations (8-10) become

$$f'''\left(1 + \left(\frac{3(n-1)}{2} W^2 (f'')^2\right)\right) + G.B\left(\frac{2m}{m+1} f'^2 - ff''\right) + G.A.M(E_1 - f'^2) = 0 \tag{14}$$

$$\theta'' + \Pr_f .E.\left(f\theta' + (A1) Nb\, \theta'\phi' + (A1) Nt\, \theta'^2 + \lambda\theta\right) = 0 \tag{15}$$

$$\phi'' + (A1).\left(\frac{1}{(A1)}\frac{Nt}{Nb}\theta'' + Lef\theta' - Le\gamma\phi\right) = 0 \tag{16}$$

$$f(\alpha) = \alpha\frac{1-m}{1+m},\ f'(\alpha) = 1, \theta(\alpha) = 1, \phi(\alpha) = 1;\ f'(\infty) = 0, \theta(\infty) = 0, \phi(\infty) = 0 \tag{17}$$

Here, $M = \frac{2\sigma_f B_0^2 (x+b)^{1-m}}{U_0(m+1)\rho_f}$ is the magnetic parameter, $W = (m+1)\frac{U_0^3 (x+b)^{3m-1}}{2\nu_f}\Gamma^2$ is the Weissenberg number, $\mathrm{Pr}_f = \frac{\mathrm{Pr}}{\left(\frac{k_{nf}}{k_f} + \frac{4}{3}R\right)}$ is the effective Prandtl number where $\mathrm{Pr} = \frac{(\mu c_p)_f}{k_f}$ is the Prandtl number, $\gamma = \frac{2K}{U_0(m+1)(x+b)^{m-1}}$ is the chemical reaction, $\mathrm{Re}_x = \frac{xU_0(x)}{\nu_f}$ - Reynolds number, $E_1 = \frac{E_0}{B_0 U_0 (x+b)^m}$ is the electric parameter, $N_b = \frac{(\rho c)_s (D_B)_f (C_w - C_\infty)}{(\rho c)_f \nu_f}$ is the Brownian motion, $N_t = \frac{(\rho c)_s (D_T)_f (T_w - T_\infty)}{(\rho c)_f \nu_f T_\infty}$ is the thermophoresis, $Le = \frac{\nu_f}{(D_B)_f}$ is the Lewis number and $R = -\frac{4\sigma^* T_\infty^3}{k_f k^*}$ is the solar radiation-conduction. Besides, the physical resources of engineering hits of materials boosting application are skin friction coefficient C_f, Nusselt number Nu_x and Sherwood number Sh_x expressed as

$$\mathrm{Re}_x^{\frac{1}{2}} C_f = \frac{1}{(1-\zeta)^{2.5}}\sqrt{\frac{m+1}{2}} f''(0),\ \mathrm{Re}_x^{-\frac{1}{2}} Nu_x = -\left(\frac{k_{nf}}{k_f} + \frac{4}{3}R\right)\sqrt{\frac{m+1}{2}}\theta'(0),\ Sh_x\,\mathrm{Re}_x^{-\frac{1}{2}} = -\frac{1}{(1-\zeta)}\sqrt{\frac{m+1}{2}}\phi'(0) \tag{17}$$

3. DISCUSSIONS

Figure 2 indicates that the magnetic field (M= 0.1,0.5, 0.9) effect with high electric field, the temperature profile decreased and such that, the temperature increased with respect to the strength of magnetic field when the electric field is weak. Table 2 shows that the rate of skin friction increases when the strengths of both electric and magnetic field are high. the heat transfer ($-\theta'(0)$) decreases in weak electric field and strong magnetic field, it is decreased but it is increasing with high electric field that means the magnetic field is dominant on the heat transfer. Table 2 shows that the concentration decreases with respect to the strength of electric field in the presence of magnetic field.

Figure 3 shows that when the wall thickness parameter increases, the temperature decreased with high and low electric field, and the thermal thickness is large. Table 3 indicates that skin friction increases with respect to the strength of the electric field. As shown in Figure 4, in weak electric field, the temperature is independent on the power-law index. Nevertheless, the change in temperature is more apparent when the electric field is strong (i.e. n=1.2, 2, 3) power law index increased no change on temperature profile with low electric field and there is slightly change when the electric field is high such that n=1.2, 2, 3. Table 4 shows that skin friction decreases with respect to the power law index when the electric field is weak and when the temperature is low. Meanwhile, the temperature increases when the thermal radiation increases low electric field in the same trend with high electric field the temperature increases and the difference between low and high electric are slightly decreased. It is interesting to note that the thermal radiation thickness is large indicating that the

nanofluid is dominated by the thermal radiation.

From Table 5, seemingly the skin friction $f''(0)$ is independent on the strength of the electric field. For the heat transfer the table shows a decrease with different electric field and an increase for the rate of mass transfer. Figure 6 indicates that the temperature change is only apparent at high Weissenberg number (i.e. We = 0.5, 1.5, 3.5). Table 4 shows that the skin friction $f''(0)$ decreases at high Weissenberg number when the electric is low with decrease in temperature $-\theta'(0)$, but increased the rate of mass transfer with different electric field.

As shown in Figure 7, the temperature drop is more apparent when electric field is strong. However, the temperature increases when the Brownian motion is significant (i.e., Nb= 0.01, 0.1, 0.3). Table 7 shows that the drop in the rate of skin friction $f''(0)$ is more apparent as the electric field is weak. In addition, the heat transfer $-\theta'(0)$increasedwith low electric and take two behaviour with high electric field. As shown in Table 7, the increase in mass transfer is more apparent when the electric field is weak. From Figure 8, the temperature increases with respect to the thermophoresis parameter in the deference electric field, is such that the deference between E1=0.0 and E1=5.0 are slightly decreased. The change in skin friction is significant when the electric field is strong. As reported in table 8, the heat transfer rate is rather low when the electric field is weak. Figure 9 shows that the temperature is independent on the Lewis parameter. On other hand the deference between the effect on Lewis parameter with low and high electric field is slightly decreased.

Table 9 indicates that the heat transfer rate $-\theta'(0)$is low in strong electric field. The mass transfer rate, however, increases with low and high electric field. Figure 10 shows no effect of low and high electric field with increased chemical reaction, and there is slight decrease with high electric field. The change in skin frictionf$''(0)$, is insignificant is strong electric field. Heat transfer drops when E1=5.0. Finally, mass transfer increases with deferent electric field. Figure 11 indicates that temperature increases as the heat source increases. On the other hand, the temperature decrease with high electric field compare with low electric field. Table 11 shows that heat transfer $-\theta'(0)$ decreases with deferent electric field. Figure 12 shows that, the prandtl parameter trend conversely. It is apparent that Prandtl parameter increases then the temperature decreases, independent on the strength of the electric field. Table 12 shows that heat transfer rate would increase if the electric field is strong.

Table 1: Thermo-Physical Properties of the Fluid and Solid Particles

	$\rho(kg/m^3)$	$c_p\ (J/kgK)$	$k(W/mK)$	$\sigma(\Omega^{-1}m^{-1})$
Pure water	997.1	4179	0.613	5.5
SWCNTs-water	2600	42.5	6600	1.26

particle shapes

Sphere, (m = 3.0) 

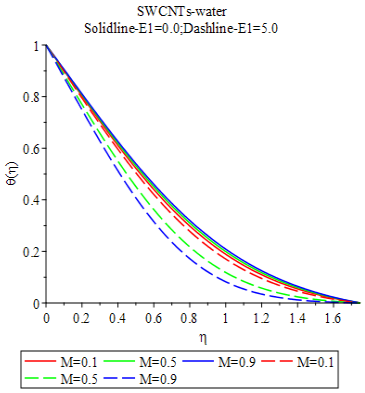

Figure 2: Magnetic Field (M)

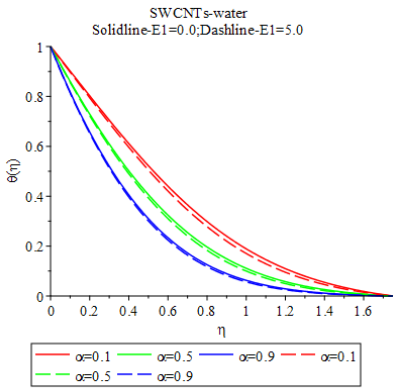

Figure 3: Wall Thickness (α)

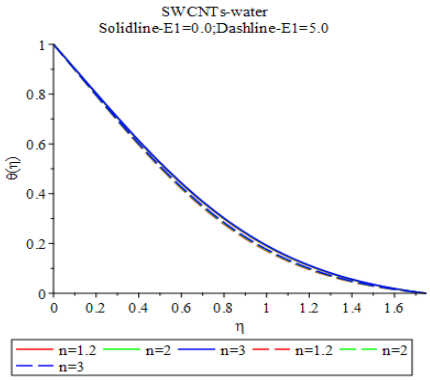

Figure 4: Effect of Power Low Index (n) on Temperature in Different Electric Fields

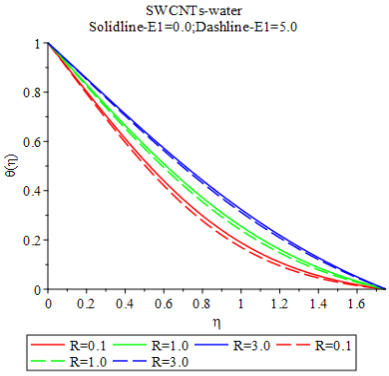

Figure 5: Thermal Radiation(R)

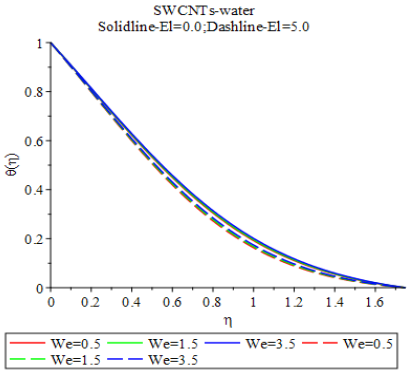

Figure 6: Weissenberg Number (W)

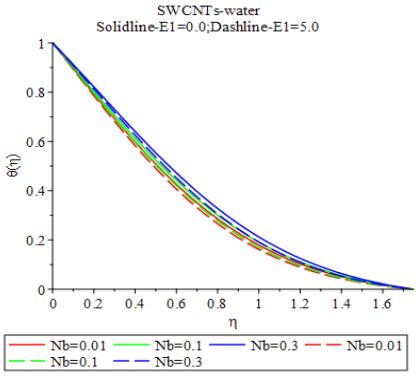

Figure 7: Effect of Brownian Motion (Nb) on Temperature in Different Electric Fields

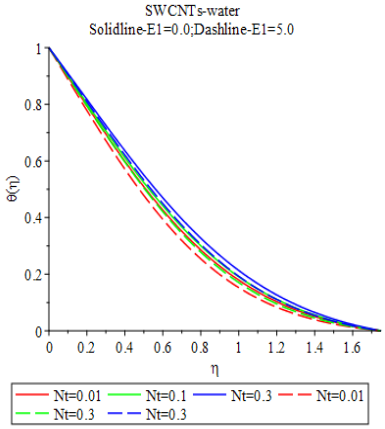

Figure 8: Thermophoresis Parameter (Nt)

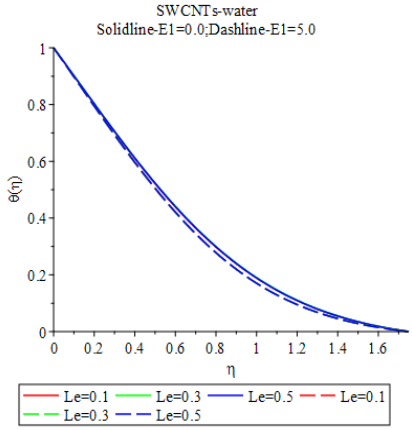

Figure 9: Lewis Number (Le)

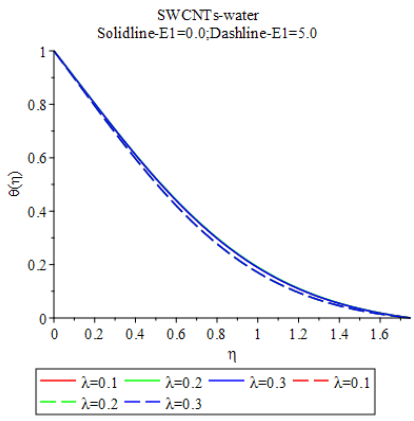

Figure 10: Effect of Chemical Reaction, on Temperature in Different Electric Fields

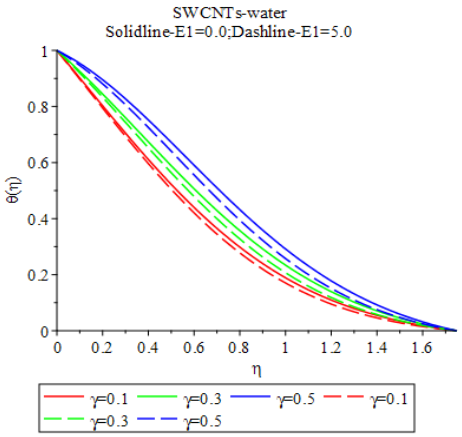

Figure 11: Heat Generation (γ)

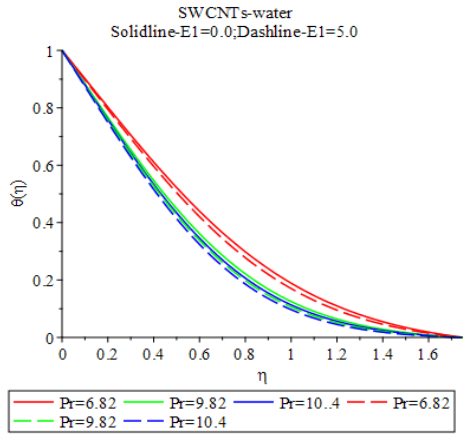

Figure 12: Effect of Parndtl Number (Pr) on Temperature in Different Electric Fields

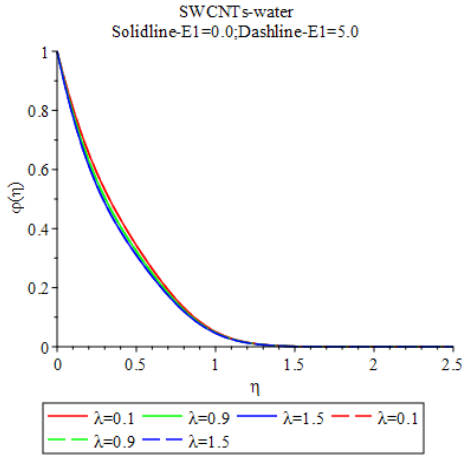

Figure 13: Companion of the Chemical Reactions Obtained from Mair Khan et al. (2017) and the Current Study

To confirm the present article with previous article, we compared the chemical reaction in articles which validates for this parameter.

Table 2: Magnetic Field Deposition on $f^{"}(0)$, $-\theta'(0)$ and $-\varphi'(0)$

M	$f^{"}(0)$	$-\theta'(0)$	$-\varphi'(0)$	Remark
0. 1	-0.06192436	0.974637508	0.135958934	E1 = 0.0
0.5	-0.21798656	0.952379683	0.151368698	
0.9	-0.35423026	0.933137979	0.164942024	
0. 1	0.206321950	1.014838665	0.109158238	E1 = 5.0
0.5	1.121600764	1.139776354	0.034226946	
0.9	2.014618856	1.244032672	0.016290443	

Table 3: The Wall Thickness Deposition on $f^{"}(0)$, $-\theta'(0)$ and $-\varphi'(0)$

α	$f^{"}(0)$	$-\theta'(0)$	$-\varphi'(0)$	Remark
0. 1	-0.06192436	0.974637508	0.135958934	E1 = 0.0
0.5	0.027429696	1.433762284	0.151368698	
0.9	-0.35423026	0.933137979	-0.25255788	
0. 1	0.098100963	1.938636067	-0.69151885	E1 = 5.0
0.5	0.206321950	1.014838665	0.109158238	
0.9	0.278513107	1.468857871	-0.27348653	

Table 4: Power Low Index Deposition on $f^{"}(0)$, $-\theta'(0)$ and $-\varphi'(0)$

n	$f^{"}(0)$	$-\theta'(0)$	$-\varphi'(0)$	Remark
1. 2	-0.06192436	0.974637508	0.135958934	E1 = 0.0
2	-0.08075871	0.970997376	0.138390665	
3	-0.35423026	0.933137979	-0.25255788	
1. 2	-0.10151830	0.967064068	0.141038574	E1 = 5.0
2	0.206321950	1.014838665	0.109158238	
3	0.172513191	1.008430946	0.113222136	

Table 5: Thermal Radiation Deposition on $f^{"}(0)$, $-\theta'(0)$ and $-\varphi'(0)$

R	$f^{"}(0)$	$-\theta'(0)$	$-\varphi'(0)$	Remark
0. 1	-0.06192436	0.974637508	0.135958934	E1 = 0.0
1.0	-0.06192437	0.833665065	0.349542219	
3.0	0.061924415	0.716012830	0.533825944	
0. 1	0.206321950	1.014838665	0.109158238	E1 = 5.0
1.0	0.206321932	0.863339187	0.331765380	
3.0	0.206321895	0.733844123	0.526822455	

Table 6: Weissenberg Number Deposition on $f^{"}(0)$, $-\theta'(0)$ and $-\varphi'(0)$

We	$f^{"}(0)$	$-\theta'(0)$	$-\varphi'(0)$	*Remark*
0. 5	-0.08075871	0.970997376	0.138390665	E1 = 0.0
1.5	-0.12009334	0.963624344	0.143371091	
3.5	-0.18103546	0.952941693	0.150710643	
0. 5	0.172513191	1.008430946	0.113222136	E1 = 5.0
1.5	0.111022612	0.996790028	0.120740391	
3.5	0.026435463	0.981229280	0.131059540	

Table 7: Brownian Motion Deposition on $f^{"}(0)$, $-\theta'(0)$ and $-\varphi'(0)$

Nb	$f^{"}(0)$	$-\theta'(0)$	$-\varphi'(0)$	*Remark*
0. 01	-0.061924362	1.027347931	-5.33031215	E1 = 0.0
0.1	-0.080758718	0.970997376	0.138390665	
0.3	-0.061924371	0.862442858	0.540802231	
0. 01	0.2063219593	1.068113220	5.682418246	E1 = 5.0
0.1	0.2063219507	1.014838665	0.109158238	
0.3	0.2063219419	0.901311372	0.538079591	

Table 8: Thermophoresis Parameter Deposition on $f^{"}(0)$, $-\theta'(0)$ and $-\varphi'(0)$

Nt	f"(0)	$-\theta'(0)$	$-\varphi'(0)$	Remark
0. 01	-0.061924370	1.017049917	0.6766383438	E1 = 0.0
0.1	-0.080758718	0.970997376	0.1383906658	
0.3	-0.061924363	0.890735511	-1.036246600	
0. 01	0.2063219532	1.112975344	0.1006663215	E1 = 5.0
0.1	0.2063219507	1.014838665	0.1091582385	
0.3	0.2063219562	0.931218226	-1.143608929	

Table 9: Lewis Number Deposition on $f^{"}(0)$, $-\theta'(0)$ and $-\varphi'(0)$

Le	$f^{"}(0)$	$-\theta'(0)$	$-\varphi'(0)$	Remark
0. 1	-0.061924368	0.981158369	0.0201155880	E1 = 0.0
0.3	-0.080758719	0.971571834	0.1277775485	
0.5	0.0619243645	0.969535715	0.2330978255	
0. 1	0.2063219488	1.022196509	-0.016019024	E1 = 5.0
0.3	0.2063219505	1.015493339	0.0976142666	
0.5	0.2063219538	1.009105399	0.2138938915	

Table 10: Chemical Reaction Deposition on $f^{"}(0)$, $-\theta'(0)$ and $-\varphi'(0)$

λ	$f^{"}(0)$	$-\theta'(0)$	$-\varphi'(0)$	Remark
0. 1	-0.061924366	0.974637508	0.1359589349	E1 = 0.0
0.2	-0.080758718	0.969968474	0.1698381885	
0.3	-0.061924366	0.972597445	0.1982995950	
0. 1	0.2063219507	1.014838665	0.1091582385	E1 = 5.0
0.2	0.2063219508	1.013761455	0.1407353665	
0.3	0.2063219509	1.012711055	0.1717381518	

Table 11: Heat Generation Deposition on $f^{"}(0)$, $-\theta'(0)$ and $-\varphi'(0)$

γ	$f^{"}(0)$	$-\theta'(0)$	$-\varphi'(0)$	Remark
0. 1	-0.061924366	0.974637508	0.1359589349	E1 = 0.0
0.3	-0.080758717	0.710446099	0.1653936047	
0.5	-0.061924363	0.396259884	0.1956959508	
0. 1	0.2063219507	1.014838665	0.1091582385	E1 = 5.0
0.3	0.2063219526	0.768525605	0.1304137086	
0.5	0.2063219546	0.470933108	0.1562449437	

Table 12: Parndtl Number Deposition on $f^{"}(0)$, $-\theta'(0)$ and $-\varphi'(0)$

Pr	$f^{"}(0)$	$-\theta'(0)$	$-\varphi'(0)$	Remark
6. 82	-0.06192436	0.974637508	0.135958934	E1 = 0.0
9.82	-0.08075871	1.153079098	-0.13255348	
10.4	-0.06192436	1.191701399	-0.18608932	
6. 82	0.206321950	1.014838665	0.109158238	E1 = 5.0
9.82	0.206321959	1.206033800	-0.16894764	
10.4	0.206321960	1.241286230	-0.22020770	

4. CONCLUSIONS

The present study was conducted to determine the effects of parameter such as thermal radiation, heat generation, thermophoresis, Brownian motion, Lewis number, magnetic field, wall thickness and power-law index on the heat transfer enhancement of nanofluid water as base fluid. The numerical solution of the first order ODEs was obtained using the Runge-Kutta Fehlberg method with shooting technique. From the converged solutions of velocity, temperature and concentration the skin friction and heat and mass transfer rates were analyzed. The following conduction can be drawn.

- The temperature decreases with respect to all parameters when the strength of the electric field is high (E1=5.0) which means the electric field is dominate of water-SWCNT.
- From the profiles of wall thickness, magnetic, radiation and heat generation strength, the thermal thickness is large. Therefore, its effect on temperature is quiet significant.
- When electric field is strong, heat transfer increases with respect to parameters such as strength of magnetic field, Parandtl number and power-law index. Meanwhile heat transfer decreases with respect to parameters such as thermal radiation, Brownian motion, thermophoresis, heat generation, chemical reaction, Lewis and Wiessenberg number.
- The results obtained from the preliminary tables show that the mass transfer rate increases with respect to electric field on thermal radiation, chemical reaction, heat generation, Lewis and Wiessenberg number.

REFERENCES

1. *S. U. S. Choi and J. A. Eastman, "Enhancing thermal conductivity of fluids with nanoparticles," Argonne National Lab., IL (United States), 1995.*
2. *W. Jiang, G. Ding, H. Peng, Y. Gao, and K. Wang, "Experimental and model research on nanorefrigerant thermal conductivity," HVAC&R Res., vol. 15, no. 3, pp. 651–669, 2009.*
3. *B. Mahar, C. Laslau, R. Yip, and Y. Sun, "Development of carbon nanotube-based sensors—a review," IEEE Sens. J., vol. 7, no. 2, pp. 266–284, 2007.*
4. *B. M. Quinn and S. G. Lemay, "Single walled carbon nanotubes as templates and interconnects for nanoelectrodes," Adv. Mater., vol. 18, no. 7, pp. 855–859, 2006.*
5. *J. Reithmaier, P. Petkov, W. Kulisch, and C. Popov, Nanostructured materials for advanced technological applications. Springer Science & Business Media, 2009.*
6. *V. N. Popov, "Carbon nanotubes: properties and application," Mater. Sci. Eng. R Reports, vol. 43, no. 3, pp. 61–102, 2004.*
7. *Sendilvelan, S., & Prabhahar, M. Pre-stress Modal Analysis of a Centrifugal Pump Impeller for Different Blade Thicknesses.*
8. *Y. Gogotsi, N. Naguib, and J. A. Libera, "In situ chemical experiments in carbon nanotubes," Chem. Phys. Lett., vol. 365, no. 3–4, pp. 354–360, 2002.*
9. *P. Lu, H. P. Lee, C. Lu, and P. Q. Zhang, "Dynamic properties of flexural beams using a nonlocal elasticity model," J. Appl. Phys., vol. 99, no. 7, p. 73510, 2006.*
10. *T. Natsuki, Q.-Q. Ni, and M. Endo, "Wave propagation in single-and double-walled carbon nanotubes filled with fluids," J. Appl. Phys., vol. 101, no. 3, p. 34319, 2007.*
11. *J. Yoon, C. Q. Ru, and A. Mioduchowski, "Vibration and instability of carbon nanotubes conveying fluid," Compos. Sci. Technol., vol. 65, no. 9, pp. 1326–1336, 2005.*
12. *C. D. Reddy, C. Lu, S. Rajendran, and K. M. Liew, "Free vibration analysis of fluid-conveying single-walled carbon nanotubes," Appl. Phys. Lett., vol. 90, no. 13, p. 133122, 2007.*
13. *E. M. Kotsalis, J. H. Walther, and P. Koumoutsakos, "Multiphase water flow inside carbon nanotubes," Int. J. Multiph. Flow, vol. 30, no. 7–8, pp. 995–1010, 2004.*
14. *L. Vaisman, H. D. Wagner, and G. Marom, "The role of surfactants in dispersion of carbon nanotubes," Adv. Colloid Interface Sci., vol. 128, pp. 37–46, 2006.*
15. *H. Wang, "Dispersing carbon nanotubes using surfactants," Curr. Opin. Colloid Interface Sci., vol. 14, no. 5, pp. 364–371, 2009.*
16. *M. Narayana and P. Sibanda, "Laminar flow of a nanoliquid film over an unsteady stretching sheet," Int. J. Heat Mass Transf., vol. 55, no. 25–26, pp. 7552–7560, 2012.*
17. *P. Cheng and W. J. Minkowycz, "Free convection about a vertical flat plate embedded in a porous medium with application to heat transfer from a dike," J. Geophys. Res., vol. 82, no. 14, pp. 2040–2044, 1977.*
18. *D. A. Nield and A. V Kuznetsov, "The Cheng–Minkowycz problem for the double-diffusive natural convective boundary layer flow in a porous medium saturated by a nanofluid," Int. J. Heat Mass Transf., vol. 54, no. 1–3, pp. 374–378, 2011.*

19. *Othman, A. A., Osman, M. A., Wahdan, M. H., & ABED-ELRAHIM, A. G. (2014). Thermal annealing and UV induced effects on the structural and optical properties of capping free ZnS nanoparticles synthesized by Co-precipitation method. International Journal of General Engineering and Technology, 3, 9-16.*

20. *M. M. Rashidi, M. Nasiri, M. S. Shadloo, and Z. Yang, "Entropy generation in a circular tube heat exchanger using nanofluids: Effects of different modeling approaches," Heat Transf. Eng., vol. 38, no. 9, pp. 853–866, 2017.*

21. *A. Karimipour, A. D'Orazio, and M. S. Shadloo, "The effects of different nano particles of Al2O3 and Ag on the MHD nano fluid flow and heat transfer in a microchannel including slip velocity and temperature jump," Phys. E Low-dimensional Syst. Nanostructures, vol. 86, pp. 146–153, 2017.*

22. *M. R. Safaei et al., "A survey on experimental and numerical studies of convection heat transfer of nanofluids inside closed conduits," Adv. Mech. Eng., vol. 8, no. 10, p. 1687814016673569, 2016.*

23. *E. Walsh, P. Walsh, R. Grimes, and V. Egan, "Thermal management of low profile electronic equipment using radial fans and heat sinks," J. Heat Transfer, vol. 130, no. 12, p. 125001, 2008.*

24. *K. Vajravelu, K. V. Prasad, and N. G. Chiu-On, "The effect of variable viscosity on the flow and heat transfer of a viscous Ag-water and Cu-water nanofluids," J. Hydrodyn. Ser. B, vol. 25, no. 1, pp. 1–9, 2013.*

25. *F. Gentile, M. Ferrari, and P. Decuzzi, "The transport of nanoparticles in blood vessels: the effect of vessel permeability and blood rheology," Ann. Biomed. Eng., vol. 36, no. 2, pp. 254–261, 2008.*

26. *S. Nadeem and S. Ijaz, "Biomechanical analysis of copper nanoparticles on blood flow through curved artery with stenosis," J. Comput. Theor. Nanosci., vol. 12, no. 9, pp. 2322–2331, 2015.*

27. *R. Ellahi, S. U. Rahman, and S. Nadeem, "Blood flow of Jeffrey fluid in a catherized tapered artery with the suspension of nanoparticles," Phys. Lett. A, vol. 378, no. 40, pp. 2973–2980, 2014.*

28. *M. J. Uddin, W. A. Khan, and N. S. Amin, "g-Jitter mixed convective slip flow of nanofluid past a permeable stretching sheet embedded in a Darcian porous media with variable viscosity," PLoS One, vol. 9, no. 6, p. e99384, 2014.*

29. *R. U. Haq, S. Nadeem, Z. H. Khan, and N. F. M. Noor, "Convective heat transfer in MHD slip flow over a stretching surface in the presence of carbon nanotubes," Phys. B Condens. matter, vol. 457, pp. 40–47, 2015.*

30. *Geete, A., & Khandwawala, A. I. (2014). Exergy analysis for 120MW thermal power plant with different inlet temperature conditions. International Journal of Research in Engineering & Technology, 2(1), 21-30.*

31. *R. Kandasamy, V. Vignesh, A. Kumar, S. H. Hasan, and N. M. Isa, "Thermal radiation energy due to SWCNTs on MHD nanofluid flow in the presence of seawater/water: Lie group transformation," Ain Shams Eng. J., 2016.*

32. *M. Khan, M. Y. Malik, and T. Salahuddin, "Heat generation and solar radiation effects on Carreau nanofluid over a stretching sheet with variable thickness: Using coefficients improved by Cash and Carp," Results Phys., vol. 7, pp. 2512–2519, 2017.*

33. *E. Magyari and A. Pantokratoras, "Note on the effect of thermal radiation in the linearized Rosseland approximation on the heat transfer characteristics of various boundary layer flows," Int. Commun. Heat Mass Transf., vol. 38, no. 5, pp. 554–556, 2011.*